NANO LETTERS

Letter

pubs.acs.org/NanoLett

Dielectric Screening of Excitons and Trions in Single-Layer MoS_2

Yuxuan Lin,*[,†] Xi Ling,[†] Lili Yu,[†] Shengxi Huang,[†] Allen L. Hsu,[†] Yi-Hsien Lee,[¶] Jing Kong,[†] Mildred S. Dresselhaus,*[,†,§] and Tomás Palacios*[,†]

[†]Department of Electrical Engineering and Computer Science, Massachusetts Institute of Technology, Cambridge, Massachusetts 02139, United States

[¶]Material Sciences and Engineering, National Tsing-Hua University, Hsinchu, 30013, Taiwan

[§]Department of Physics, Massachusetts Institute of Technology, Cambridge, Massachusetts 02139, United States

Supporting Information

ABSTRACT: Photoluminescence (PL) properties of single-layer MoS_2 are indicated to have strong correlations with the surrounding dielectric environment. Blue shifts of up to 40 meV of exciton or trion PL peaks were observed as a function of the dielectric constant of the environment. These results can be explained by the dielectric screening effect of the Coulomb potential; based on this, a scaling relationship was developed with the extracted electronic band gap and exciton and trion binding energies in good agreement with theoretical estimations. It was also observed that the trion/exciton intensity ratio can be tuned by at least 1 order of magnitude with different dielectric environments. Our findings are helpful to better understand the tightly bound exciton properties in strongly quantum-confined systems and provide a simple approach to the selective and separate generation of excitons or trions with potential applications in excitonic interconnects and valleytronics.

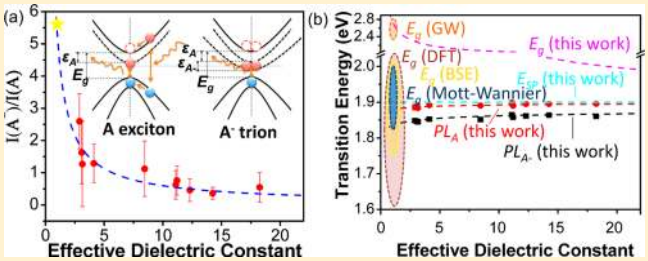

KEYWORDS: *Transition metal dichalcogenides, molybdenum disulfide, exciton, photoluminescence, dielectric screening, binding energy*

Layered transition metal dichalcogenides (LTMDs) have raised considerable attention on theoretical and experimental aspects[1−5] due to their unique electronic[1,4,6−20] and optical properties[4,14,15,21−32] with potential applications in electronics[4,5,33−37] and high-performance optoelectronics,[21,22,38,39] especially when thinned down to several atoms thick. Quantum confinement effects distinguish the single-layer semiconducting LTMDs, such as MoS_2, $MoSe_2$, WS_2, and WSe_2, from their bulk counterparts in various aspects, including indirect-to-direct band gap transition,[7,8,23,24] large exciton binding energy,[9,10,15,25] abundance of multiexcitons,[26−28] susceptibleness to the surrounding dielectrics,[16−18] and so forth. The impact of the dielectric environment to these single-layer LTMD systems is worth in-depth research. First of all, dielectrics have to be involved and considered in almost every fundamental study or application of low-dimensional materials with high surface-to-volume ratio. Furthermore, it has been reported that many-body effects,[10−15,25,40,41] which mainly result from strong electron−electron or electron−hole Coulomb interactions, play important roles in electronic transport and optical transitions in single-layer semiconducting LTMDs; such Coulomb interactions are strongly coupled with the dielectric properties of the surrounding materials, which is also known as the dielectric screening effect.[40−43] Therefore, the optical transitions, which reflect the behaviors of excitons (a bound state of one electron and one hole) or trions (a bound state of either two electrons and one hole, or one electron and two holes, also called charged excitons), should be intensively influenced by the screening of the dielectric environment.

Environmental dielectrics have been found to strongly influence both the electrical and optical properties of low dimensional materials, including quantum wells, carbon nanotubes, graphene, and so forth.[40−45] However, such study on LTMDs is still in its early stage.[16−18,46−51] Several groups have studied the mobility enhancement effect of MoS_2 field effect transistors by introducing a gate oxide with higher dielectric constants,[16−18] and they have explained this enhancement as the screening of long-range Coulomb interactions induced by impurity charges. In terms of the optical properties, several groups studied the Raman and PL spectra of atomicly thin MoS_2 layers on various solid substrates,[47−51] and they attributed the shift of the PL peaks to either doping or strain induced by the dielectric or metallic substrates. In those systems, however, the effect of dielectric screening on the exciton-related optical transitions was not considered.

In this work, the intrinsic influence of the dielectric constant of the environments on the exciton behaviors of single-layer MoS_2 is investigated. To prevent the doping or strain effect that may be induced by the fabrication process or the lattice mismatch between MoS_2 and the dielectrics, we use nonionic

Received: May 28, 2014
Revised: September 3, 2014
Published: September 12, 2014

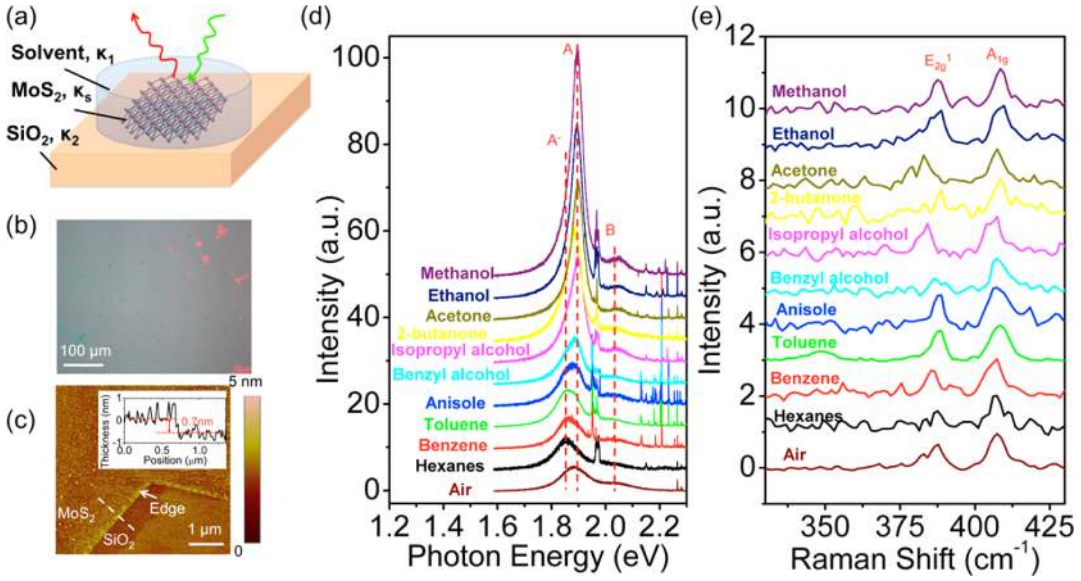

Figure 1. (a) Schematic of the experimental setup. The CVD MoS_2 is on a SiO_2/Si substrate and immersed in a specific organic, nonionic solvent. The relative dielectric constants of the MoS_2, the solvent, and the substrate layer are denoted by κ_s, κ_1, and κ_2, respectively. (b) Optical microscopic image of CVD MoS_2 grown on the SiO_2/Si substrate. (c) AFM image of CVD MoS_2 grown on the SiO_2/Si substrate. The inset is the height profile plotted along the white dashed line. The step height, or the thickness of the MoS_2, is around 0.7 nm, indicating that the MoS_2 is single-layer. (d) Photoluminescence and (e) Raman spectra of single-layer MoS_2 exposed to air or immersed in different solvents. The spectra are arranged by an ascending order (from bottom to top) according to the dielectric constant of the solvents. The wavelength of the excitation laser is 532.5 nm.

organic solvents as the environmental dielectrics,[44−46] having the relative dielectric constants from 2 to 33. Blue shifts of the PL peaks of up to 40 meV were observed as a function of the dielectric constant of the solvent. The PL peaks were thereby enhanced and narrowed accordingly, and the trion/exciton intensity ratio can thus be tuned by a large amount as well. The shifts can be attributed to the dielectric screening of the Coulomb interactions either between electrons and holes, or between different electrons that can affect the binding energies of excitons and trions or the quasiparticle electronic band structures of the MoS_2. The binding energies of excitons and trions in single-layer MoS_2 with both surfaces in vacuum were extracted to be around 900 and 40 meV, respectively, and the electronic band gap to be around 2.7 eV, in good agreement with recent theoretical predictions.[9−15,25,52] The large tuning of the trion/exciton intensity ratio by the solvent can be explained by the mass action model. This effect provides a simple method to generate excitons and trions separately and selectively, which paves the way to studying the behaviors of excitons and trions independently, and to potentially realizing well-controlled excitonic interconnects[53] and high-efficiency valleytronics.[29−31]

Figure 1a shows a schematic diagram of the device. Continuous single-layer MoS_2 was grown on 300 nm SiO_2/Si substrates by chemical vapor deposition (CVD) with the assistance of perylene-3,4,9,10-tetracarboxylic acid tetrapotassium salt (PTAS) as the seeding promoter.[54−56] The optical microscopic image of the MoS_2-on-SiO_2 sample is shown in Figure 1b. The atomic force microscopic (AFM) image shown in Figure 1c indicates that the surface of the as-grown MoS_2 is smooth and clean, and the height profile (inset) along the dotted line in the AFM image confirms that the MoS_2 is single layer with a thickness of around 0.7 nm. The sample was then immersed in different nonionic organic solvents with a static relative dielectric constant (κ_1) from 2 to 33 and PL and Raman spectroscopy measurements were carried out on it. The spectroscopy measurements were taken on a confocal microscopic setup with the excitation laser wavelength of 532.5 nm. The solvents include hexanes (κ_1 = 1.89), benzene (κ_1 = 2.28), toluene (κ_1 = 2.38), anisole (κ_1 = 4.33), benzyl alcohol (κ_1 = 13), isopropyl alcohol (κ_1 = 18.3), 2-butanone (κ_1 = 18.5), acetone (κ_1 = 20.7), ethanol (κ_1 = 24.6), and methanol (κ_1 = 32.6).[57] More properties of these solvents can be found in Supporting Information. The reasons for choosing these organic, nonionic solvents are that any ions in the solvents, if any, may dope MoS_2, which can influence the PL and Raman spectra as well, and that these solvents should not react with MoS_2. Because the samples were successively immersed in different solvents during the measurement, it is necessary to check the quality of MoS_2 after each solvent-immersed measurement. In order to do this, after each spectroscopy measurement of the MoS_2 sample in one of these solvents the sample was taken out and rinsed with acetone and isopropyl alcohol and another measurement was carried out on the sample in air. The PL peak positions of the sample exposed to air did not change much before and after in contact with any of the solvents, as shown in Figure S1 in the Supporting Information, indicating that neither the chemical reactions nor physical attachments changed the excitonic properties of MoS_2 when immersed in the solvents. As the PL and Raman spectra vary with the position of the laser beam spot on the sample, we took the average of 5−10 spectra collected with different beam positions throughout the sample for each dielectric configuration.

Figure 1d,e show typical PL and Raman spectra, respectively, of single-layer MoS_2 with the bottom surface in contact with the SiO_2/Si substrate, while the top surface is exposed to air or to different solvents. The PL spectra can be fitted with three Lorentzian peaks with the peak positions located at around 1.85, 1.90, and 2.03 eV, respectively. More fitting details are provided in Supporting Information Figure S2. The multiple sharp peaks in Figure 1d are from the Raman vibrational modes of the solvent, MoS_2, or the SiO_2/Si substrate. The assignments

dx.doi.org/10.1021/nl501988y | Nano Lett. 2014, 14, 5569−5576

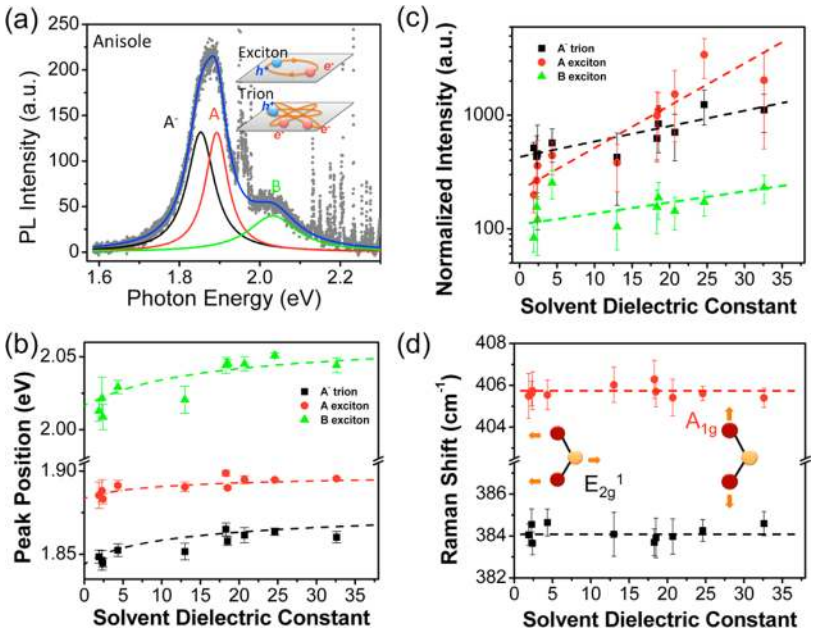

Figure 2. (a) A typical PL spectrum of single-layer MoS_2 that is immersed in anisole. The gray dots are experimental data, and the black, red, and green lines are the three fitted peaks by Lorenztian functions. The blue line is the summation of the fitting peaks, which matches the experimental data very well. The inset schematics demonstrate the classical pictures of a trion and an exciton, which are bound states of 2 electrons with 1 hole, and 1 electron with 1 hole, respectively. (b) The PL peak positions as a function of the solvent dielectric constant. The dots with error bars are experimental data, and the dashed curves are fitting curves from the scaling relationship. (c) Accumulated PL intensities normalized to the A_{1g} Raman peak intensities with the dots together with their error bars showing experimental data and the dashed lines are the guides to the eye. (d) Raman shifts of the E_{2g}^1 and A_{1g} vibrational modes as a function of the solvent dielectric constant. The inset schematics indicate the directions of the vibration of each atom for each mode.

of these peaks are shown in Supporting Information Figure S6. Figure 1e shows the Raman spectra of MoS_2 with the in-plane vibrational mode, E_{2g}^1, and the out-of-plane vibrational mode, A_{1g}, located at around 385 and 407 cm^{-1}, respectively.

In Figure 2a, a typical PL spectrum in one of the solvents (anisole) was fitted with three peaks, which have been assigned to originate from the radiative combination of the A^- trion (~1.85 eV), A exciton (~1.90 eV), and B exciton (~2.03 eV), respectively.[26,58] We notice that the intensity of the A^- trion peak (black curve) is comparable with the intensity of the A exciton (red curve). The strong radiative recombination of trions in LTMD materials is consistent with the study published elsewhere.[26,27] The peak positions, accumulated intensities normalized by the A_{1g} Raman peak intensities, and full widths at half-maximum (fwhm) of all three PL peaks as a function of the dielectric constant of the solvents are plotted in Figure 2b,c and Supporting Information Figure S7, respectively. From Figure 2b, it is observed that the energy positions of all the three peaks increase as the dielectric constant of the solvent increases, whereas these blue shifts start to saturate when the dielectric constant exceeds 18. Note that the A^- trion peak shifts faster than the A exciton peak, and the energy difference between the A^- trion and the A exciton peak, that is, the trion binding energy, becomes very small in high-κ solvents. The intensities of the PL peaks are enhanced approximately exponentially as a function of the dielectric constant of the solvent, as shown in Figure 2c, where the PL intensities versus dielectric constant is plotted on a log scale. The A^- trion peak is enhanced by ~4 times, the A exciton peak by ~20 times, and the B exciton peak by less than 2 times. There is also a negative correlation between the peak widths and the dielectric constant of the solvent for all three peaks, according to the plots shown in Supporting Information Figure S7.

To quantify the screening effect on the excitons and trions in single-layer MoS_2 by the external dielectrics from our results, we would like to exclude other possible environmental factors that may also influence the electron-to-photon transition energies, including temperature,[26,27] mechanical strain,[19,59] doping,[26,60] interference effect, and so forth. The laser power was kept sufficiently low (less than 2.2 $mW/\mu m^2$) to avoid the heating of MoS_2. From Raman spectroscopy measurements, if the solvents induce any strain[59] or doping[60] effect in the MoS_2 the E_{2g}^1 and A_{1g} Raman vibrational modes would shift. However, none of these were observed in our data, as shown in Figure 2d. There is no clear dependence of the intensities and widths of the Raman modes on the type of solvents as well, which are given in Figure S8 and S9 in the Supporting Information. Therefore, we can neglect any doping or strain induced by the solvents. However, it is highly possible that the effect of the charge transfer could affect the PL of single-layer MoS_2 if it is exposed to air. Figure 1d also shows the PL spectrum of MoS_2 when exposed to ambient. The three PL peaks of MoS_2 are located at 1.85, 1.89, and 2.03 eV, respectively; yet the dielectric constant of air is 1, and from the trend generalized from Figure 2b,c, the PL peaks of single-layer MoS_2 in air should have the lowest peak energies, and the weakest peak intensities. To understand this unexpected observation, PL and Raman spectra were taken on MoS_2 in vacuum, and a comparison was made with those taken in air. The PL and Raman spectra of single-layer MoS_2 in vacuum (less than 10^{-4} Torr) are distinct from those in air, as shown in Supporting Information Figure S10. The PL peaks of single-layer MoS_2 measured in vacuum are located at around 1.77,

dx.doi.org/10.1021/nl501988y | Nano Lett. 2014, 14, 5569−5576

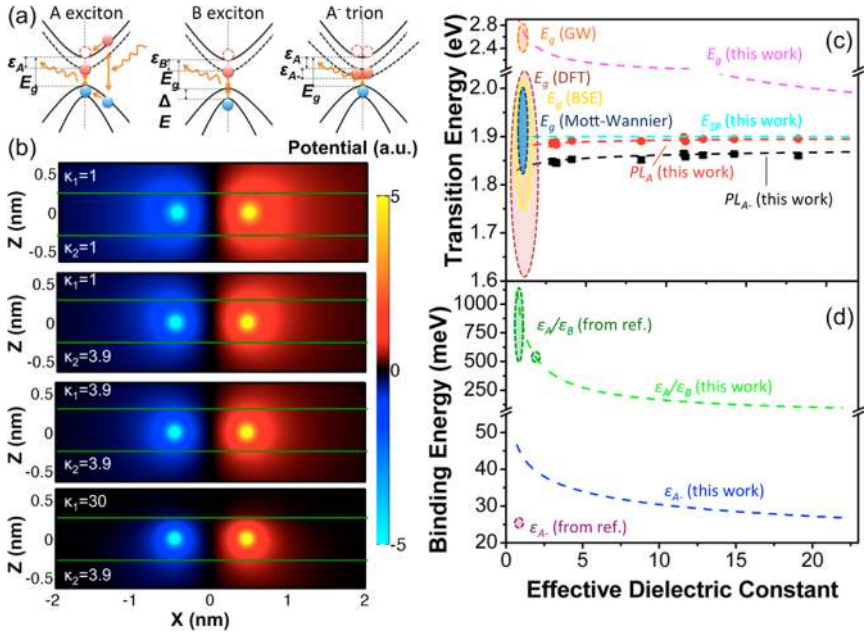

Figure 3. (a) Schematics of the exciton-related radiative transition at the *K* -point in the Brillioun zone. E_g, Δ, ε_A, ε_B, ε_{A-} denote the band gap, valence band splitting, binding energy of the A, B exciton and A^- trion, respectively. (b) Coulomb potential distribution with a positive and a negative unit charge in the middle layer of the dielectric-sandwich structure. The four contours are for different dielectric configurations. (c) Dependence of the PL peak energies of the A exciton (PL_A, red) and A^- trion (PL_{A-}, black), the electronic band gap (E_g, magenta), the band gap based on the single-particle picture (E_{SP}, cyan) on the effective dielectric constant. The dots with error bars are experimental data, and the dotted lines are the fitting results from the binding energy scaling relationship. (d) Dependence of the binding energies of the A/B exciton (green) and A^- trion (blue) on the effective dielectric constant. In (c,d), the shaded areas with different colors are the calculated results by other groups.[9−15,52]

1.83, and 1.95 eV, respectively, and the peak intensities are much smaller than that measured in air. These observations are in accordance with the trend obtained from the solvent-based PL data. This difference of the peaks in air and in vacuum may be attributed to the carrier depletion effects induced by the p-type doping of MoS_2 by the water and other high-electronegativity molecules present in air and absorbed by the anion vacancy defects,[61] which helps to enhance the quantum yield of the PL process when MoS_2 is in air. The intensity ratio of the A_{1g} and $E_{2g}{}^1$ Raman modes is also smaller when MoS_2 is in vacuum than in air, as shown in the inset of Supporting Information Figure S10. This trend is a further indication of the existence of the p-doping effect, as has been observed in electrochemically gated MoS_2.[60] Finally, the interference effect on the incident and excited light introduced by the Solvent/MoS_2/SiO_2/Si structure was examined. According to Li et al.,[62] an interference enhancement factor should be considered in the total PL intensity if the dielectric configuration changes. However, this enhancement factor only varies by less than 20% throughout our measurements when different solvents are used as the external dielectrics, and these small changes are far below the enhancement (>10 times) observed in the experiment (Figure 1d). Therefore, the interference effect should have negligible contributions to the tuning of the PL intensities.

The PL peak energy of direct-bandgap semiconductors, usually called the optical band gap, is equal to the electronic band gap calculated from the electronic dispersion relation minus the binding energy of the quasiparticles (excitons or trions) originating from the Coulomb interactions between the electrons and holes. In the case of single-layer MoS_2, the three peak energies can be expressed as $PL_A = E_g - \varepsilon_A$, $PL_B = E_g + \Delta - \varepsilon_B$, $PL_{A-} = E_g - \varepsilon_A - \varepsilon_{A-}$, respectively, where E_g is the electronic direct band gap of single-layer MoS_2, Δ is the valence band splitting at the *K*-point in the Brillioun zone originating from the spin−orbit coupling,[24] and ε_A, ε_B, and ε_{A-} are the binding energies of the A exciton, B exciton, and A^- trion, respectively. The band diagrams of the three quasiparticles are schematically shown in Figure 3a. The binding energies of the quasiparticles reflect the Coulomb interaction between the negatively charged electrons and the positively charged holes, which can be calculated through the reduced-mass hydrogen atom model in the 2D case.[9,63] However, the Coulomb potential distribution is strongly screened by the environmental dielectrics. Figure 3b and Figures S12 and S13 in the Supporting Information show the Coulomb potential distributions of the electron−hole pair in the dielectrics/MoS_2/dielectrics structure. The relative dielectric constants of the top and bottom dielectric layers are denoted as κ_1 and κ_2, respectively. The impact of the boundary conditions on the Coulomb potential distributions due to the dielectric mismatch is equivalent to the generation of an infinite array of image charges. The net potential of the image charges diminishes the total potential if the environmental dielectric constants κ_1 and κ_2 are larger than the MoS_2 dielectric constant κ_s, and strengthens the total potential if κ_1 and κ_2 are smaller. The dielectric-screened Coulomb potential for the electron and hole separated by a distance *L* can be expressed as

$$V_{2D}(L) = \frac{e^2}{\varepsilon_0 \kappa_{eff} L_0} f\left(\frac{L}{L_0}\right)$$

where ε_0 and *e* are the vacuum permittivity and the electron charge, $\kappa_{eff} = (\kappa_1 + \kappa_2)/2$ is the effective relative dielectric constant, and L_0 is the screening length, $f(L/L_0)$ is a dimensionless function, and the detailed expressions are given

dx.doi.org/10.1021/nl501988y | Nano Lett. 2014, 14, 5569−5576

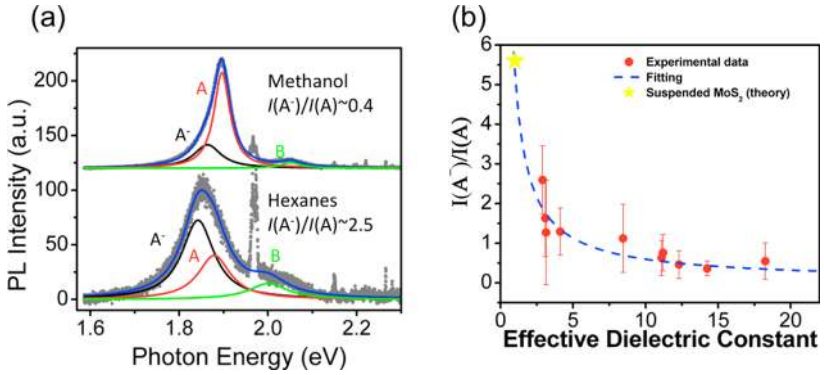

Figure 4. (a) PL spectra of single-layer MoS_2 immersed in methanol and hexanes, respectively. Gray dots are experimental data, and the black, red, and green lines are the fitting curves of the peaks of the A^- trion, A exciton, and B exciton, respectively, with the blue line the summation of the three fitting curves. (b) Dependence of the A^-/A intensity ratio on the effective dielectric constant. The red dots with error bars are experimental data, and the blue dotted line is the fitting results from the mass action model. The yellow star is the estimated intensity ratio of suspended MoS_2 with both surfaces in vacuum according to our model.

in ref 25. Similar to the method used by Perebeinos et al.,[40] the exciton binding energy has the following scaling relationship:

$$\varepsilon_X = \varepsilon_{X0}(\kappa_{eff})^{-\alpha_X}$$

where ε_{X0} is the exciton binding energy in vacuum, and α_X is the empirical scaling factor. Here X stands for A, B, or A^-. We assume that the A and B excitons should have similar behaviors, because the only difference between the A and B excitons is that the holes are from the two separated valence bands.[23,24] Therefore, the fitting parameters of A and B should be close to each other, that is, $\alpha_A \approx \alpha_B$ and $\varepsilon_{A0} \approx \varepsilon_{B0}$. According to Berghäuser et al.,[13] the binding energies of A and B excitons are 860 and 870 meV in vacuum and 455 and 465 meV with one surface in contact with SiO_2, respectively, which is consistent with our assumption. These values were used as fixed parameters in our fitting. The binding energy of the A^- trion (ε_{A-}) should follow the same power law, except that the scaling factor α_{A-} may have a distinct value. On the other hand, the electron−electron interaction, or the electron self-energy should also be influenced by dielectric screening in a similar way as the electron−hole interaction. This electron self-energy adds a renormalization term to the electronic band gap, which has been reported to be prominent in low-dimensional systems, especially in LTMDs.[9−15,52] As a result, the quasiparticle electronic band gap can be given by

$$E_{gX} = E_{SPX} + E_{BGRX} = E_{SPX} + \frac{E_{BGRX0}}{(\kappa_{eff})^{\beta_X}}$$

where E_{SPX} and E_{BGRX} are the electronic band gap from the single-particle model, and the electron self-energy band gap renormalization term, respectively, while X stands for A or B, indicating different subbands. Following the similar scaling relationship, E_{BGRX} can be further expressed by the renormalization term in vacuum, denoted as E_{BGRX0}, divided by the power function of κ_{eff} with the scaling parameter β_X. Note that $E_g = E_{gA}$, and $\Delta = E_{gB} - E_{gA}$. Therefore, the PL peak energies of A, B exciton and A^- trion are given by

$$PL_A = E_g - \frac{\varepsilon_{A0}}{(\kappa_{eff})^{\alpha_A}} = E_{SPA} + \frac{E_{BGRA0}}{(\kappa_{eff})^{\beta_A}} - \frac{\varepsilon_{A0}}{(\kappa_{eff})^{\alpha_A}}$$

$$PL_B = E_g + \Delta - \frac{\varepsilon_{B0}}{(\kappa_{eff})^{\alpha_B}} = E_{SPB} + \frac{E_{BGRB0}}{(\kappa_{eff})^{\beta_B}} - \frac{\varepsilon_{B0}}{(\kappa_{eff})^{\alpha_B}}$$

$$PL_{A-} = E_g - \frac{\varepsilon_{A0}}{(\kappa_{eff})^{\alpha_A}} - \frac{\varepsilon_{A-,0}}{(\kappa_{eff})^{\alpha_{A-}}}$$
$$= E_{SPA} + \frac{E_{BGRA0}}{(\kappa_{eff})^{\beta_A}} - \frac{\varepsilon_{A0}}{(\kappa_{eff})^{\alpha_A}} - \frac{\varepsilon_{A-,0}}{(\kappa_{eff})^{\alpha_{A-}}}$$

Figure 2b shows in dashed lines the PL peak energies as a function of the dielectric constant of the solvents fitted by the expressions mentioned above. The fitting results match the experimental data very well. Figure 3c plots the electronic band gap, single-particle band gap, the A exciton and A^- trion PL peak positions, and Figure 3 d plots the relative binding energies of the A and B excitons and of the A^- trion as a function of the effective dielectric constant. Both the electronic band gap and the exciton binding energies are relatively large when MoS_2 is in vacuum and decrease rapidly with the effective dielectric constant. The PL peak positions, or optical band gaps of the excitonic quasiparticles are the differences between those energies; thus the large changes cancel out mostly, leading to small changes of the PL peak positions as a function of the dielectric constant. In an extreme case, if the effective dielectric approaches infinity, both the electron self-energy renormalization and the excitonic binding energies are infinitesimal, and the optical band gaps are close to the single-particle band gap. The binding energies of the A, B exciton and A^- trion with both surfaces in vacuum are extracted to be 859, 870, and 44 meV, respectively. The electronic band gap of single-layer MoS_2 in vacuum is around 2.73 eV. Figure 3c also summarizes the reported values from different calculation methods in the literature. Density functional theory (DFT) calculations provide the band structure without considering the electron−electron interactions. The calculated band gap from the DFT method, ranging from 1.6 to 2.1 eV,[10,11,14,52] should be equal to E_{SP} (~1.90 eV) according to our model. The many-body GW perturbation theory includes the effect of the electron−electron interaction with the calculated band gap of 2.4−2.8 eV[9−15,52] and the excitonic effect can be considered by using the Mott−Wannier theory or solving the Bethe−Salpeter equation (BSE), which gives the binding energy of 500−1100 meV,[9,10,12−15,25] and the optical band gap of 1.74−2.0 eV,[9,14,15,52] respectively. The estimated values based on our model are in good agreement with these calculations. The valence band splitting at the *K*-point is estimated to be 172 meV, very close to theoretical anticipations[9−11,13,14] and previous PL and

dx.doi.org/10.1021/nl501988y | *Nano Lett.* 2014, 14, 5569−5576

absorption measurements.[23,24] Supporting Information Figure S14 shows the dependence of the valence band splitting on the effective dielectric constant. The scaling factors in our fittings are $\alpha_A = 0.7 \pm 0.2$, $\alpha_B = 0.7 \pm 0.2$, $\alpha_{A-} = 0.16 \pm 0.06$, $\beta_A = 0.7 \pm 0.2$ and $\beta_B = 0.8 \pm 0.2$.

From Figure 2c, we observe that the peak intensities of the A, B excitons and A^- trions increase exponentially with the solvent dielectric constant. It is also noted that the peak widths decrease with the solvent dielectric constant, according to Supporting Information Figure S7. Given that the PL peak width is inversely proportional to the lifetime of the quasiparticles, we can infer that the lifetimes of the excitons and trions in single-layer MoS_2 become larger when immersed in high-κ dielectric environments. As we can see in Figure 3b, the Coulomb potential becomes more confined within the middle layer if the dielectric constants of the top and bottom layers are higher. This may help to reduce the scattering between the excitons (trions) and the charged impurities at the MoS_2/dielectrics interface,[16−18] and thus prolong the lifetime of the excitons (trions). As a result, the quantum efficiency of the excitonic recombination process becomes larger when MoS_2 is in high-κ environments. This explains the enhancement of the PL intensities of MoS_2 by high-κ dielectrics. However, the nonradiative recombination rate of the excitons is still so high that the lifetime of excitons in single-layer MoS_2 is only about 80 ps, according to Shi et al.[32] Because of this, the excitons and trions may have very low mobility and, consequently, a very slow response to the electric field change. This explains why there is no clear correlation between the PL spectra and the high-frequency dielectric constant of the solvents as shown in Supporting Information Figure S15. Here the high-frequency dielectric constant is defined as the square of the refractive index of the solvent in the visible range.

The intensity ratio of trions and excitons can be tuned by the environmental dielectric constant as well. As shown in Figure 4a, the A^-/A intensity ratio decreases from 2.5 to 0.4 as the effective dielectric constant varies from 3 to 20 (or the solvent dielectric constant from 1.89 to 32.6). From the mass action model, the trion/exciton intensity ratio can be expressed as

$$\frac{I(A^-)}{I(A)} = \frac{\Gamma_{A-} N_{A-}}{\Gamma_A N_A} \propto \frac{\Gamma_{A-}}{\Gamma_A} \frac{1}{n_e} \exp\left(\frac{\varepsilon_{A-}}{k_B T}\right)$$

where Γ_{A-} and Γ_A are the radiative recombination rates, and N_{A-} and N_A are the density of A^- and A, respectively; n_e is the electron density; and $k_B T = 25.9$ meV is the thermal energy at room temperature (300 K). More information on the mass action model is provided in the Supporting Information. The radiative recombination should be influenced by the environmental dielectrics as well, similar to other low-dimensional systems;[43,64,65] thus the ratio of the A^-/A radiative recombination rate (inverse of the radiative lifetime) is assumed to follow the power function of the effective dielectric constant; that is, $\Gamma_{A-}/\Gamma_A \propto (\kappa_{eff})^{\delta}$. Therefore, the A^-/A intensity ratio is given by

$$\frac{I(A^-)}{I(A)} = K(\kappa_{eff})^{\delta} \exp\left(\frac{\varepsilon_{A-}}{k_B T}\right)$$

with the fitting parameters K and δ. Figure 4b shows the fitting results compared with the experimental data. The scaling factor δ here is extracted to be around −0.7, meaning that the radiative recombination rate of the A exciton changes faster with the environmental dielectric constant than that of the A^- trion. This model gives an estimation of the electron density of $\sim 10^{12}$ cm^{-2}, which is in good agreement with the values reported by others.[16,20,58] From the mass action model, we can expect that the A^-/A intensity ratio can be as high as 5.5 if both sides of MoS_2 are exposed to vacuum ($\kappa_1 = \kappa_2 = 1$), or as low as 0.10 if MoS_2 are exposed to an ultrahigh-κ dielectric (for example, $\kappa_1 = \kappa_2 = 100$).

In summary, we provided an in-depth understanding of the effect of dielectric screening on the excitonic dynamics in single-layer MoS_2. To explain the PL features tuned by the surrounding dielectric environments, a simple scaling relationship derived from the dielectric-screened Coulomb potential and effective-mass approximation was developed. The electronic band gap, the valence band splitting, the exciton and trion binding energies were extracted and the results yield reasonable values, which are helpful to understand the excitonic behaviors in strongly quantum-confined 2D LTMDs. Furthermore, the A exciton and A^- trion can be generated separately and selectively, using specific surrounding dielectrics configurations. This phenomenon provides a simple approach both to independently studying the behaviors of excitons and trions, and to potentially realizing well-controlled excitonic interconnects and high-efficiency valleytronics.

■ ASSOCIATED CONTENT

Supporting Information

Experimental method, PL spectra fitting details, basic properties of the organic solvents, additional results on PL and Raman spectroscopy of solvent-immersed single-layer MoS_2, and details used in the modeling and fitting. This material is available free of charge via the Internet at http://pubs.acs.org.

■ AUTHOR INFORMATION

Corresponding Authors

*E-mail: (Y.L.) liny@mit.edu.
*E-mail: (M.S.D.) millie@mgm.mit.edu.
*E-mail: (T.P.) tpalacios@mit.edu.

Notes

The authors declare no competing financial interest.

■ ACKNOWLEDGMENTS

The authors acknowledge the support by ONR PECASE 6926686, NSF/DMR-1004147, NSF/DMR-1231319, and EFRC-33TEC. The authors are grateful to Professor Mark Baldo, Professor Humberto Terrones, Xu Zhang, Qiong Ma, Joaquin Rodriguez Nieva, and Alexandre Rocha Paschoal for useful discussions.

■ REFERENCES

(1) Novoselov, K. S.; Jiang, D.; Schedin, F.; Booth, T. J.; Khotkevich, V. V.; Morozov, S. V.; Geim, A. K. Two-dimensional atomic crystals. *Proc. Natl. Acad. Sci. U.S.A.* **2005**, *102*, 10451.

(2) Nicolosi, V.; Chhowalla, M.; Kanatzidis, M. G.; Strano, M. S.; Coleman, J. N. Liquid Exfoliation of Layered Materials. *Science* **2013**, *340*, 1226419.

(3) Chhowalla, M.; Shin, H. S.; Eda, G.; Li, L.-J.; Loh, K. P.; Zhang, H. The chemistry of two-dimensional layered transition metal dichalcogenide nanosheets. *Nat. Chem.* **2013**, *5*, 263.

(4) Wang, Q. H.; Kalantar-Zadeh, K.; Kis, A.; Coleman, J. N.; Strano, M. S. Electronics and optoelectronics of two-dimensional transition metal dichalcogenides. *Nat. Nanotechnol.* **2012**, *7*, 699.

(5) Hsu, A.; Wang, H.; Shin, Y. C.; Mailly, B.; Zhang, X.; Yu, L.; Shi, Y.; Lee, Y. H.; Dubey, M.; Kim, K. K.; Kong, J.; Palacios, T. Large-Area 2-D Electronics: Materials, Technology, and Devices. *Proc. IEEE* **2013**, *101*, 1638.
(6) Zhu, W.; Low, T.; Lee, Y.-H.; Wang, H.; Farmer, D. B.; Kong, J.; Xia, F.; Avouris, P. Electronic transport and device prospects of monolayer molybdenum disulphide grown by chemical vapour deposition. *Nat. Commun.* **2014**, *5*, 3087.
(7) Zhang, Y.; Chang, T.-R.; Zhou, B.; Cui, Y.-T.; Yan, H.; Liu, Z.; Schmitt, F.; Lee, J.; Moore, R.; Chen, Y.; Lin, H.; Jeng, H.-T.; Mo, S.-K.; Hussain, Z.; Bansil, A.; Shen, Z.-X. Direct observation of the transition from indirect to direct bandgap in atomically thin epitaxial $MoSe_2$. *Nat. Nanotechnol.* **2014**, *9*, 111.
(8) Jin, W.; Yeh, P.-C.; Zaki, N.; Zhang, D.; Sadowski, J. T.; Al-Mahboob, A.; van der Zande, A. M.; Chenet, D. A.; Dadap, J. I.; Herman, I. P.; Sutter, P.; Hone, J.; Osgood, R. M. Direct Measurement of the Thickness-Dependent Electronic Band Structure of MoS_2 Using Angle-Resolved Photoemission Spectroscopy. *Phys. Rev. Lett.* **2013**, *111*, 106801.
(9) Cheiwchanchamnangij, T.; Lambrecht, W. R. L. Quasiparticle band structure calculation of monolayer, bilayer, and bulk MoS_2. *Phys. Rev. B* **2012**, *85*, 205302.
(10) Qiu, D. Y.; da Jornada, F. H.; Louie, S. G. Optical Spectrum of MoS_2: Many-Body Effects and Diversity of Exciton States. *Phys. Rev. Lett.* **2013**, *111*, 216805.
(11) Molina-Sánchez, A.; Sangalli, D.; Hummer, K.; Marini, A.; Wirtz, L. Effect of spin-orbit interaction on the optical spectra of single-layer, double-layer, and bulk MoS_2. *Phys. Rev. B* **2013**, *88*, 045412.
(12) Hüser, F.; Olsen, T.; Thygesen, K. S. How dielectric screening in two-dimensional crystals affects the convergence of excited-state calculations: Monolayer MoS_2. *Phys. Rev. B* **2013**, *88*, 245309.
(13) Berghäuser, G.; Malic, E. Analytical approach to excitonic properties of MoS_2. *Phys. Rev. B* **2014**, *89*, 125309.
(14) Ramasubramaniam, A. Large excitonic effects in monolayers of molybdenum and tungsten dichalcogenides. *Phys. Rev. B* **2012**, *86*, 115409.
(15) Komsa, H.-P.; Krasheninnikov, A. V. Effects of confinement and environment on the electronic structure and exciton binding energy of MoS_2 from first principles. *Phys. Rev. B* **2012**, *86*, 241201.
(16) Radisavljevic, B.; Kis, A. Mobility engineering and a metal–insulator transition in monolayer MoS_2. *Nat. Mater.* **2013**, *12*, 815.
(17) Li, S.-L.; Wakabayashi, K.; Xu, Y.; Nakaharai, S.; Komatsu, K.; Li, W.-W.; Lin, Y.-F.; Aparecido-Ferreira, A.; Tsukagoshi, K. Thickness-Dependent Interfacial Coulomb Scattering in Atomically Thin Field-Effect Transistors. *Nano Lett.* **2013**, *13*, 3546.
(18) Ma, N.; Jena, D. Charge Scattering and Mobility in Atomically Thin Semiconductors. *Phys. Rev. X* **2013**, *4*, 011043.
(19) Conley, H. J.; Wang, B.; Ziegler, J. I.; Haglund, R. F.; Pantelides, S. T.; Bolotin, K. I. Bandgap Engineering of Strained Monolayer and Bilayer MoS_2. *Nano Lett.* **2013**, *13*, 3626.
(20) Baugher, B. W. H.; Churchill, H. O. H.; Yang, Y.; Jarillo-Herrero, P. Intrinsic Electronic Transport Properties of High-Quality Monolayer and Bilayer MoS_2. *Nano Lett.* **2013**, *13*, 4212.
(21) Lopez-Sanchez, O.; Lembke, D.; Kayci, M.; Radenovic, A.; Kis, A. Ultrasensitive photodetectors based on monolayer MoS_2. *Nat. Nanotechnol.* **2013**, *8*, 497.
(22) Sundaram, R. S.; Engel, M.; Lombardo, A.; Krupke, R.; Ferrari, A. C.; Avouris, P.; Steiner, M. Electroluminescence in Single Layer MoS_2. *Nano Lett.* **2013**, *13*, 1416.
(23) Mak, K. F.; Lee, C.; Hone, J.; Shan, J.; Heinz, T. F. Atomically Thin MoS_2: A New Direct-Gap Semiconductor. *Phys. Rev. Lett.* **2010**, *105*, 136805.
(24) Splendiani, A.; Sun, L.; Zhang, Y.; Li, T.; Kim, J.; Chim, C.-Y.; Galli, G.; Wang, F. Emerging Photoluminescence in Monolayer MoS_2. *Nano Lett.* **2010**, *10*, 1271.
(25) Berkelbach, T. C.; Hybertsen, M. S.; Reichman, D. R. Theory of neutral and charged excitons in monolayer transition metal dichalcogenides. *Phys. Rev. B* **2013**, *88*, 045318.
(26) Mak, K. F.; He, K.; Lee, C.; Lee, G. H.; Hone, J.; Heinz, T. F.; Shan, J. Tightly bound trions in monolayer MoS_2. *Nat. Mater.* **2013**, *12*, 207.
(27) Ross, J. S.; Wu, S.; Yu, H.; Ghimire, N. J.; Jones, A. M.; Aivazian, G.; Yan, J.; Mandrus, D. G.; Xiao, D.; Yao, W.; Xu, X. Electrical control of neutral and charged excitons in a monolayer semiconductor. *Nat. Commun.* **2013**, *4*, 1474.
(28) Sie, E. J.; Lee, Y.-H.; Frenzel, A. J.; Kong, J.; Gedik, N. *Biexciton formation in monolayer MoS_2 observed by transient absorption spectroscopy*. **2013** arXiv:1312.2918 [cond-mat].
(29) Mak, K. F.; He, K.; Shan, J.; Heinz, T. F. Control of valley polarization in monolayer MoS_2 by optical helicity. *Nat. Nanotechnol.* **2012**, *7*, 494.
(30) Zeng, H.; Dai, J.; Yao, W.; Xiao, D.; Cui, X. Valley polarization in MoS_2 monolayers by optical pumping. *Nat. Nanotechn.* **2012**, *7*, 490.
(31) Mai, C.; Barrette, A.; Yu, Y.; Semenov, Y. G.; Kim, K. W.; Cao, L.; Gundogdu, K. Many-Body Effects in Valleytronics: Direct Measurement of Valley Lifetimes in Single-Layer MoS_2. *Nano Lett.* **2014**, *14*, 202.
(32) Shi, H.; Yan, R.; Bertolazzi, S.; Brivio, J.; Gao, B.; Kis, A.; Jena, D.; Xing, H. G.; Huang, L. Exciton Dynamics in Suspended Monolayer and Few-Layer MoS_2 2D Crystals. *ACS Nano* **2013**, *7*, 1072.
(33) Radisavljevic, B.; Radenovic, A.; Brivio, J.; Giacometti, V.; Kis, A. Single-layer MoS_2 transistors. *Nat. Nanotechnol.* **2011**, *6*, 147.
(34) Wang, H.; Yu, L.; Lee, Y.-H.; Shi, Y.; Hsu, A.; Chin, M. L.; Li, L.-J.; Dubey, M.; Kong, J.; Palacios, T. Integrated Circuits Based on Bilayer MoS_2 Transistors. *Nano Lett.* **2012**, *12*, 4674.
(35) Radisavljevic, B.; Whitwick, M. B.; Kis, A. Integrated Circuits and Logic Operations Based on Single-Layer MoS_2. *ACS Nano* **2011**, *5*, 9934.
(36) Wang, H.; Yu, L.; Lee, Y.; Fang, W.; Hsu, A.; Herring, P.; Chin, M.; Dubey, M.; Li, L.; Kong, J.; Palacios, T. Large-scale 2D electronics based on single-layer MoS_2 grown by chemical vapor deposition. *IEEE Int. Electron Devices Meet.* **2012**, DOI: 10.1109/IEDM.2012.6478980.
(37) Fang, H.; Chuang, S.; Chang, T. C.; Takei, K.; Takahashi, T.; Javey, A. High-Performance Single Layered WSe_2 p-FETs with Chemically Doped Contacts. *Nano Lett.* **2012**, *12*, 3788.
(38) Roy, K.; Padmanabhan, M.; Goswami, S.; Sai, T. P.; Ramalingam, G.; Raghavan, S.; Ghosh, A. Graphene-MoS_2 hybrid structures for multifunctional photoresponsive memory devices. *Nat. Nanotechnol.* **2013**, *8*, 826.
(39) Ross, J. S.; Klement, P.; Jones, A. M.; Ghimire, N. J.; Yan, J.; Mandrus, D. G.; Taniguchi, T.; Watanabe, K.; Kitamura, K.; Yao, W.; Cobden, D. H.; Xu, X. Electrically Tunable Excitonic Light Emitting Diodes based on Monolayer WSe_2 p-n Junctions. *Nat. Nanotechnol.* **2013**, *9*, 268.
(40) Perebeinos, V.; Tersoff, J.; Avouris, P. Scaling of Excitons in Carbon Nanotubes. *Phys. Rev. Lett.* **2004**, *92*, 257402.
(41) Walsh, A. G.; Nickolas Vamivakas, A.; Yin, Y.; Cronin, S. B.; Selim Ünlü, M.; Goldberg, B. B.; Swan, A. K. Scaling of exciton binding energy with external dielectric function in carbon nanotubes. *Phys. E* **2008**, *40*, 2375.
(42) Kumagai, M.; Takagahara, T. Excitonic and nonlinear-optical properties of dielectric quantum-well structures. *Phys. Rev. B* **1989**, *40*, 12359.
(43) Kulik, L. V.; Kulakovskii, V. D.; Bayer, M.; Forchel, A.; Gippius, N. A.; Tikhodeev, S. G. Dielectric enhancement of excitons in near-surface quantum wells. *Phys. Rev. B* **1996**, *54*, R2335.
(44) Newaz, A. K. M.; Puzyrev, Y. S.; Wang, B.; Pantelides, S. T.; Bolotin, K. I. Probing charge scattering mechanisms in suspended graphene by varying its dielectric environment. *Nat. Commun.* **2012**, *3*, 734.
(45) Chen, F.; Xia, J.; Ferry, D. K.; Tao, N. Dielectric screening enhanced performance in graphene FET. *Nano Lett.* **2009**, *9*, 2571.
(46) Mao, N.; Chen, Y.; Liu, D.; Zhang, J.; Xie, L. Solvatochromic effect on the photoluminescence of MoS_2 monolayers. *Small* **2013**, *9*, 1312.
(47) Yan, R.; Bertolazzi, S.; Brivio, J.; Fang, T.; Konar, A.; Birdwell, A. G.; Nguyen, N. V.; Kis, A.; Jena, D.; Xing, H. G. Raman and

Photoluminescence Study of Dielectric and Thermal Effects on Atomically Thin MoS_2. 2012 arXiv:1211.4136 [cond-mat].
(48) Buscema, M.; Steele, G. A.; van der Zant, H. S. J.; Castellanos-Gomez, A. The effect of the substrate on the Raman and photoluminescence emission of single layer MoS_2. *Nano Res.* **2014**, *7*, 561.
(49) Sercombe, D.; Schwarz, S.; Del Pozo-Zamudio, O.; Liu, F.; Robinson, B. J.; Chekhovich, E. A.; Tartakovskii, I. I.; Kolosov, O.; Tartakovskii, A. I. Optical investigation of the natural electron doping in thin MoS_2 films deposited on dielectric substrates. *Sci. Rep.* **2013**, *3*, 3489.
(50) Scheuschner, N.; Ochedowski, O.; Kaulitz, A.-M.; Gillen, R.; Schleberger, M.; Maultzsch, J. Photoluminescence of freestanding single- and few-layer MoS_2. *Phys. Rev. B* **2014**, *89*, 125406.
(51) Plechinger, G.; Schrettenbrunner, F.-X.; Eroms, J.; Weiss, D.; Schüller, C.; Korn, T. Low-temperature photoluminescence of oxide-covered single-layer MoS_2. *Physica Status Solidi (RRL)* **2012**, *6*, 126.
(52) Feng, J.; Qian, X.; Huang, C.-W.; Li, J. Strain-engineered artificial atom as a broad-spectrum solar energy funnel. *Nat. Photonics* **2012**, *6*, 866.
(53) Baldo, M.; Stojanović, V. Optical switching: Excitonic interconnects. *Nat. Photonics* **2009**, *3*, 558.
(54) Lee, Y.-H.; Zhang, X.-Q.; Zhang, W.; Chang, M.-T.; Lin, C.-T.; Chang, K.-D.; Yu, Y.-C.; Wang, J. T.-W.; Chang, C.-S.; Li, L.-J.; Lin, T.-W. Synthesis of Large-Area MoS_2 Atomic Layers with Chemical Vapor Deposition. *Adv. Mater.* **2012**, *24*, 2320.
(55) Lee, Y.-H.; Yu, L.; Wang, H.; Fang, W.; Ling, X.; Shi, Y.; Lin, C.-T.; Huang, J.-K.; Chang, M.-T.; Chang, C.-S.; Dresselhaus, M.; Palacios, T.; Li, L.-J.; Kong, J. Synthesis and Transfer of Single-Layer Transition Metal Disulfides on Diverse Surfaces. *Nano Lett.* **2013**, *13*, 1852.
(56) Ling, X.; Lee, Y.-H.; Lin, Y.; Fang, W.; Yu, L.; Dresselhaus, M. S.; Kong, J. Role of the Seeding Promoter in MoS_2 Growth by Chemical Vapor Deposition. *Nano Lett.* **2014**, *14*, 464.
(57) http://www.hbcpnetbase.com/ (accessed May 9, 2014).
(58) Mouri, S.; Miyauchi, Y.; Matsuda, K. Tunable Photoluminescence of Monolayer MoS_2 via Chemical Doping. *Nano Lett.* **2013**, *13*, 5944.
(59) Rice, C.; Young, R. J.; Zan, R.; Bangert, U.; Wolverson, D.; Georgiou, T.; Jalil, R.; Novoselov, K. S. Raman-scattering measurements and first-principles calculations of strain-induced phonon shifts in monolayer MoS_2. *Phys. Rev. B* **2013**, *87*, 081307.
(60) Chakraborty, B.; Bera, A.; Muthu, D. V. S.; Bhowmick, S.; Waghmare, U. V.; Sood, A. K. Symmetry-dependent phonon renormalization in monolayer MoS_2 transistor. *Phys. Rev. B* **2012**, *85*, 161403.
(61) Tongay, S.; Suh, J.; Ataca, C.; Fan, W.; Luce, A.; Kang, J. S.; Liu, J.; Ko, C.; Raghunathanan, R.; Zhou, J.; Ogletree, F.; Li, J.; Grossman, J. C.; Wu, J. Defects activated photoluminescence in two-dimensional semiconductors: interplay between bound, charged, and free excitons. *Sci. Rep.* **2013**, *3*, 2657.
(62) Li, S.-L.; Miyazaki, H.; Song, H.; Kuramochi, H.; Nakaharai, S.; Tsukagoshi, K. Quantitative Raman Spectrum and Reliable Thickness Identification for Atomic Layers on Insulating Substrates. *ACS Nano* **2012**, *6*, 7381.
(63) Yang, X. L.; Guo, S. H.; Chan, F. T.; Wong, K. W.; Ching, W. Y. Analytic solution of a two-dimensional hydrogen atom. I. Nonrelativistic theory. *Phys. Rev. A* **1991**, *43*, 1186.
(64) Califano, M.; Franceschetti, A.; Zunger, A. Lifetime and polarization of the radiative decay of excitons, biexcitons, and trions in CdSe nanocrystal quantum dots. *Phys. Rev. B* **2007**, *75*, 115401.
(65) Ohno, Y.; Maruyama, S.; Mizutani, T. Environmental effects on photoluminescence of single-walled carbon nanotubes. Carbon Nanotubes. *InTech* **2010**, DOI: 10.5772/39421.